Geophysical Research Letters®

Key Points:

- Notable differences exist in Holocene land surface temperature (LST) variations on the Chinese Loess Plateau
- Rainfall-induced changes in surface vegetation dynamics modulated LST changes
- Surface vegetation changes contribute to the Holocene temperature controversies

Correspondence to:

H. X. Lu and W. G. Liu,
luhx@ieecas.cn;
liuwg@loess.llqg.ac.cn

Author Contributions:

Conceptualization: W. G. Liu
Formal analysis: Z. H. Liu, Y. B. Sun, H. Y. Wang, Z. Wang, J. B. Dong, M. Xing, S. G. Kang, H. Liu, X. Liu, W. J. Sheng, Y. N. Cao, J. Hu
Methodology: W. G. Liu
Writing – review & editing: W. G. Liu, Z. H. Liu, Y. B. Sun, H. Y. Wang, Z. Wang, J. B. Dong, M. Xing, S. G. Kang, H. Liu

Vegetation-Driven Spatial Heterogeneity of Land Surface Temperature Changes on the Chinese Loess Plateau

H. X. Lu[1] , W. G. Liu[1] , Z. H. Liu[1,2], Y. B. Sun[1] , H. Y. Wang[1] , Z. Wang[1] , J. B. Dong[1] , M. Xing[1] , S. G. Kang[1], H. Liu[1], X. Liu[3], W. J. Sheng[1], Y. N. Cao[1], and J. Hu[1]

[1]State Key Laboratory of Loess Science, Institute of Earth Environment, Chinese Academy of Sciences, Xi'an, China, [2]Department of Earth Sciences, The University of Hong Kong, Hong Kong, China, [3]Xi'an Institute for Innovative Earth Environment Research, Xi'an, China

Abstract A comprehensive understanding of the processes and mechanisms driving Holocene temperature changes is crucial for resolving the ongoing Holocene temperature controversy. Here, we reconstructed land surface temperature (LST) variations over the past 27,000 years in two loess-paleosol profiles from the Chinese Loess Plateau based on soil bacterial lipid signatures. By combining our data with other published records derived from the same proxy, we identify notable spatial inconsistencies in LST trends across geographically proximate areas with distinct vegetation cover, despite the expectation that air temperature trends should be consistent. By integrating modern meteorological data, we propose that rainfall-induced changes in surface vegetation dynamics are a key factor contributing to this divergence. This contributes to our understanding of past climate dynamics in East Asia and underscores the importance of considering vegetation effects when interpreting paleoclimate data and resolving controversies over Holocene temperature trends.

Plain Language Summary Land-atmosphere interactions are crucial for understanding how regional temperatures change. Here, we looked at land surface temperature (LST) changes by analyzing soil bacterial markers. We found that LST trends varied notably across regions that were close to each other but had different types of vegetation. In the southern and eastern Chinese Loess Plateau (CLP), where vegetation is more abundant, LST changes generally matched patterns of magnetic properties of the soil, organic carbon content, and regional air temperatures. However, in the northern and western CLP, where vegetation is sparse, LSTs showed noticeable differences from air temperatures, with higher LSTs during the Last Glacial Maximum and lower LSTs during the middle Holocene. These spatial differences suggest that regional vegetation variations played a key role in the temperature changes we observed. Our findings are further supported by modern meteorological records, which demonstrate that the influence of vegetation on the temperature disparity between LSTs and air temperatures intensifies as rainfall and vegetation cover decrease, especially when rainfall is less than 600 mm. This study highlights the important role of vegetation in historical LST changes and helps us better understand Holocene temperature trends and land-atmosphere interactions in East Asia.

1. Introduction

As the most recent interglacial period, the Holocene offers a crucial time window for evaluating current global warming and projecting future temperature changes. Therefore, it has attracted widespread attention from scientists and various sectors of society. However, discrepancies in the reconstructed Holocene temperature changes have been observed among different indicators, even for the same indicator in different areas or similar areas (Chen et al., 2023). One important factor contributing to these discrepancies is the complexity of land-atmosphere interactions. Land surface processes, such as vegetation, soil moisture, and land use changes, along with the feedback mechanisms between these processes and the atmosphere, can have notable impacts on local land surface temperatures (LSTs) (Chen et al., 2024; Piao et al., 2019; Shen et al., 2015). For example, deforestation can lead to changes in albedo and surface roughness, affecting the energy balance and atmospheric circulation, resulting in differential changes between LSTs and atmospheric temperatures (Bonan, 2008).

However, quantifying the impact of land-atmosphere interactions on Holocene temperature changes is challenging due to: (a) data limitations, as climate proxies have issues with spatial coverage, temporal resolution, and accuracy; (b) the combined effect of multiple driving forces like solar radiation, ice volume, and greenhouse gases, which complicate isolating land-atmosphere contributions (Huybers, 2006; Kaufman et al., 2004; Petit et al., 1999); and (c) the lack of precise land temperature indicators, as many proxies are influenced by both
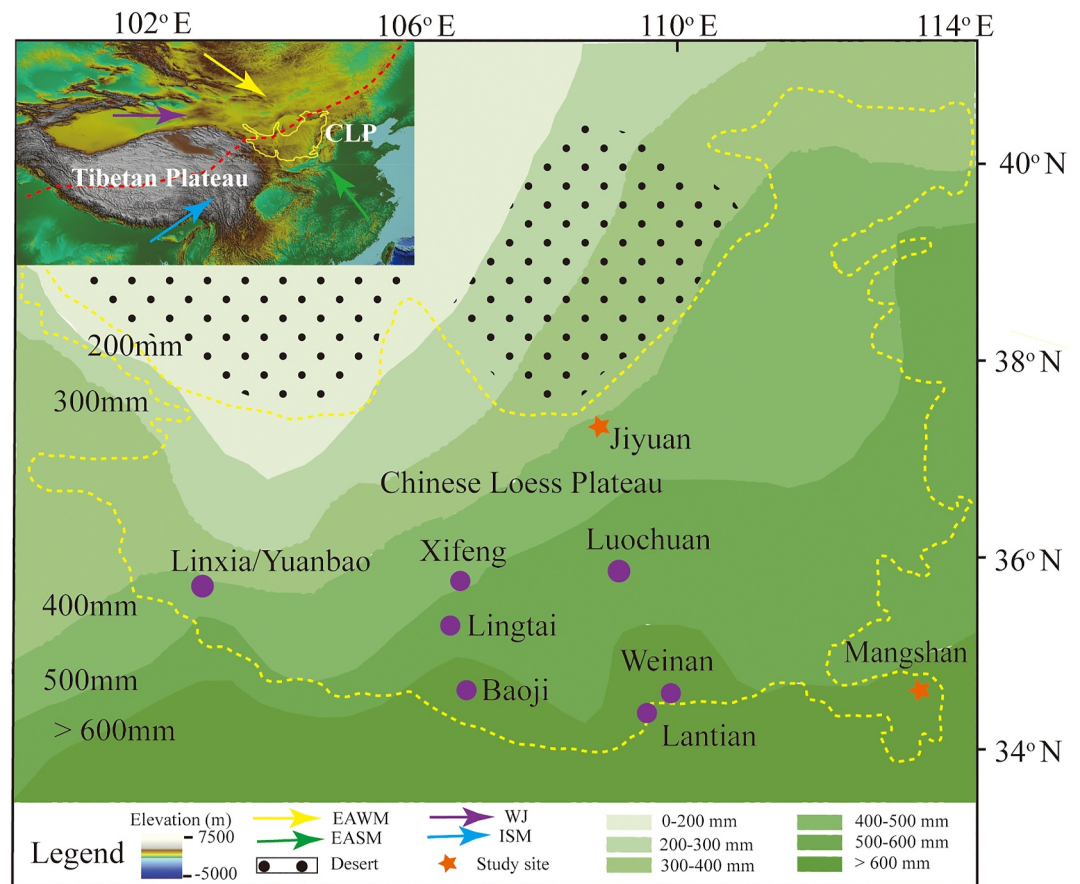
Figure 1. Geographic locations of loess–paleosol sections on the Chinese Loess Plateau (CLP) (purple dots, previous studies; orange stars, this study) and surrounding deserts. The area enclosed in yellow dash lines denotes the CLP. The modern mean annual precipitation isohyets were modified after Guo et al. (2022). The inset map illustrates the position of the CLP in relation to the Tibetan Plateau and the current Asian atmospheric circulation system. The orange dotted line represents the boundary of the Asian summer monsoon (Chen et al., 2019). EASM, East Asian summer monsoon; EAWM, East Asian winter monsoon; WJ, Westerly jet; ISM, Indian summer monsoon.

temperature and precipitation (Guo et al., 2024, 2025). Chinese loess-paleosol sequence, which has garnered global attention (An et al., 1991, 2000), is poised to offer fresh insights into this challenge. These loess profiles, with wide distributions and geographical proximity, show notable spatial variations in vegetation cover and soil moisture (H. C. Jiang & Ding, 2005; Xin et al., 2008). Moreover, microbial lipid branched glycerol dialkyl glycerol tetraethers (brGDGTs, see Figure S1 in Supporting Information S1 for structures), recognized as robust terrestrial paleothermometers (H. Y. Wang et al., 2020; Weijers et al., 2006, 2007), have been widely identified in loess across the CLP (Gao et al., 2012; Guo et al., 2024; Lu et al., 2019, 2022; Peterse et al., 2011, 2014; Thomas et al., 2017). However, most records are from central and southern CLP, with low resolution and chronological uncertainty (Figure 1). In addition, soil moisture could impact brGDGT-temperature calibrations (Dang et al., 2016). A new regional temperature calibration, based on modern soil brGDGTs and in situ temperatures, can potentially correct the impact of soil moisture, offering a more reliable LST variation sequence (H. Y. Wang et al., 2020).

Obtaining high-resolution and dependable temperature records is crucial for advancing our comprehension of how spatial variations in vegetation impact LST changes. In this study, we meticulously selected two representative loess-paleosol profiles with accurate chronological information and varying vegetation coverage from the southern and northern regions of the CLP. By reconstructing their LST dynamics over the past 27,000 years, we aimed to evaluate the spatial variability in LSTs, particularly focusing on the Holocene period. Our analysis revealed notable spatial heterogeneity in the LST trends, likely attributable to differences in changes in surface

vegetation coverage, a finding supported by contemporary observational data. These insights offer novel perspectives that enhance our understanding of Holocene land temperature changes.

2. Materials and Methods

The loess samples were collected from two well-known classic loess profiles (Mangshan, 34°57′N, 113°22′E) and Jiyuan (37°6′N, 107°22′E) (Figure 1) at the southeastern and northern CLP (Text S1 in Supporting Information S1). The current mean air temperatures (MATs) at these two locations are 15.0°C and 8.7°C, respectively, while the mean annual precipitation (MAP) amounts are 645 and 328 mm per year, respectively (Figure S2 in Supporting Information S1). We applied the conventional single-aliquot regenerative-dose optical stimulated luminescence (OSL) dating protocol to fine quartz grains (4–11 μm) from the Mangshan and Jiyuan 2 loess sections, as described by Kang et al. (2020) (Figure S3 and Text S2 in Supporting Information S1). GDGTs were analyzed using a liquid chromatography/atmospheric pressure chemical ionization-mass spectrometry system (Text S3 in Supporting Information S1).

3. Results and Discussion

3.1. Spatiotemporal Pattern of LST Variations in the CLP

BrGDGTs are widely acknowledged as robust terrestrial paleothermometers and have been extensively utilized in reconstructing paleotemperature across the CLP (Peterse et al., 2011, 2014; Tang et al., 2017; Thomas et al., 2017) (see Text S3 in Supporting Information S1 for brGDGTs distribution and the fidelity of the brGDGTs paleotemperatures). LSTs varied from 20.1°C to 26.1°C (mean 23.3°C) at Mangshan, −2.3°C–15.8°C (mean 6.6°C) at Jiyuan 1, and 5.9°C–17.3°C (mean 11.6°C) at Jiyuan 2. LST changes were most significant at Jiyuan 1 (18.1°C), followed by Jiyuan 2 (11.4°C) and Mangshan (6.0°C) (Figure 2). The magnitude of LST changes varied greatly, with 18.1°C at the Jiyuan 1 section, 11.4°C at the Jiyuan 2 section (the Holocene only), and 6.0°C at the Mangshan section. Notably, the use of different temperature empirical calibrations can greatly impact the reconstructed absolute temperature values, however it does not affect the overall structure (Figure S4 in Supporting Information S1). Spatially, we note an obvious increasing trend in the timing of early warming from the south Mangshan to north Jiyuan during the last glacial/deglacial period. Warming commenced at Jiyuan before ~25 ka, followed by Mangshan at ~20 ka (Figure 2). This increasing early and prolonged warming pattern toward the northwestern plateau at the onset of deglaciation is consistent with our previous finding (Figure S5 in Supporting Information S1) (Lu et al., 2019). Consequently, there exist notable regional disparities in temperature variations (Figure 2). The LSTs across the eastern and southern CLPs were lower during the Last Glacial Maximum (LGM) and higher during the mid-Holocene, which was generally consistent with the intensity of solar radiation and East Asian Summer Monsoon (EASM) circulation during the same period (Figure 2). For the western and northern CLP, however, LGM temperatures were higher, even surpassed those during the mid-Holocene.

Holocene temperature records from the CLP reveal surprising spatial patterns. On the southern and eastern CLPs with substantial vegetation coverage, LSTs during the mid-Holocene were relatively high, which is highly consistent with the total organic carbon content, regional integrated air temperature (Fang & Hou, 2011; S. W. Wang & Gong, 2000) (Figure S6 in Supporting Information S1), as well as the East Asian summer monsoon (EASM) intensity recorded by magnetic susceptibility and the oxygen isotope composition ($\delta^{18}O$) of cave speleothems from southeast China (Cheng et al., 2016) (Figure 2). Indeed, the mid-Holocene is considered a warm benchmark period for climate simulations in East Asia, supported by various geological records (Bentley et al., 2009; Li et al., 2018; Yang et al., 2011). In addition, the loess units are generally interpreted to reflect more arid conditions, whereas paleosols are thought to document more humid conditions, which is consistent with the higher temperature reconstructed in the paleosol layer. In contrast, the Jiyuan section of the northern CLP, with sparse vegetation, experienced unexpected cooling during the mid-Holocene, even cooler than LGM temperatures. This cooling, confirmed by the Linxia record (Guo et al., 2024) (Figure 2), contrasts with other climate indicators (Figure S6 in Supporting Information S1), indicating a unique climatic response in this region.

The temporal and spatial inconsistency of Holocene temperature changes have been attributed to various forcing mechanisms, including seasonal insolation changes, ice sheets, greenhouse gas concentrations, and ocean overturning circulation (Andersen et al., 2004; Bova et al., 2021; Kaufman et al., 2004, 2020; Lin et al., 2024; Marchal et al., 2002; Marcott et al., 2013; T. X. Wang et al., 2023). However, these factors may not fully explain
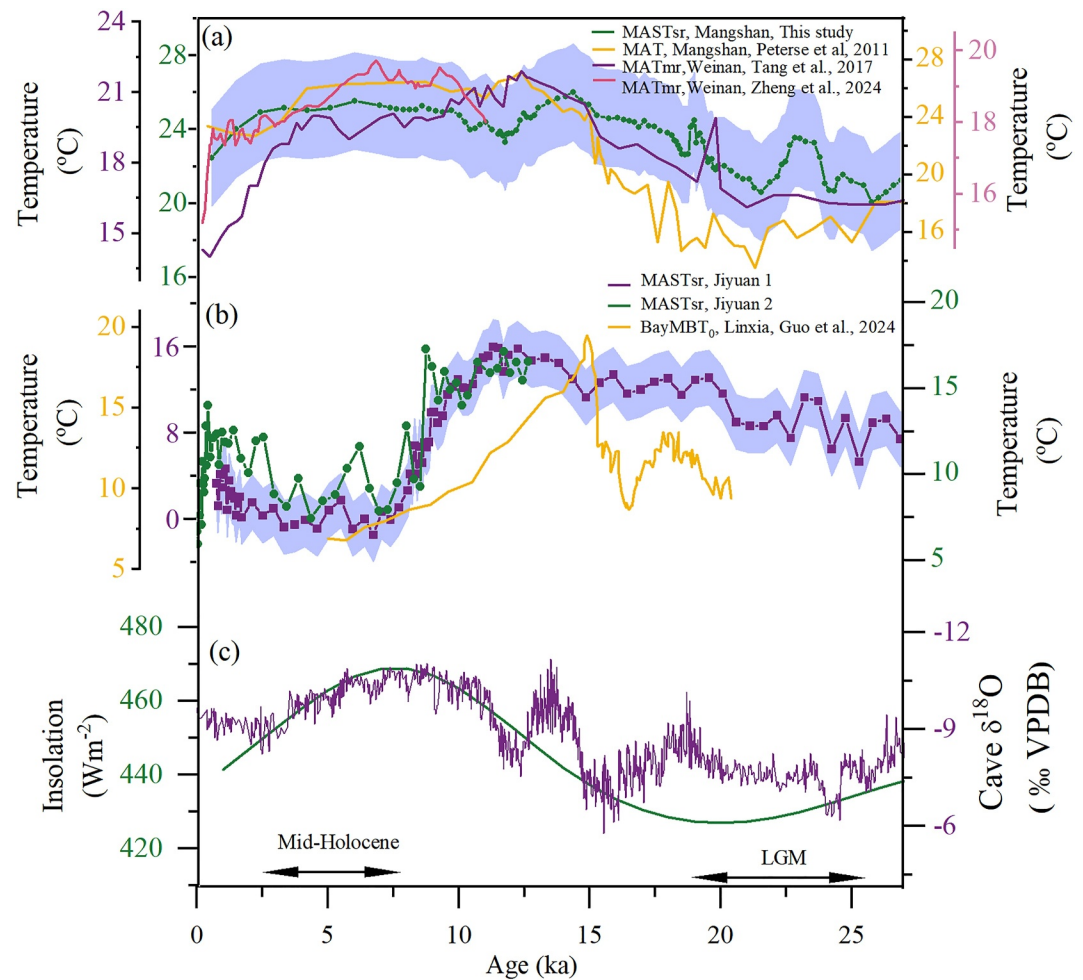
Figure 2. Comparison of land surface temperature (LST) records derived from brGDGTs from the Chinese Loess Plateau (CLP) and other paleo-records over the past 27 Kyr. (a) LSTs for the southern and eastern CLP with higher MAP and better vegetation coverage (green, Mangshan, three-point averaged $MAST_{sr}$, this study; yellow, Mangshan, three-point averaged MAT, Peterse et al., 2011; purple, Weinan, MAT_{mr}, Tang et al., 2017; pink, Weinan, MAT_{mr}, Zheng et al., 2024). (b) LSTs for the northern and western CLP with lower MAP and poor vegetation coverage (green and purple, Jiyuan Sections 1 and 2, $MAST_{sr}$, this study; yellow, Linxia, $BayMBT_0$, Guo et al., 2024). (c) EASM as indicated by $\delta^{18}O$ of stacked speleothem records from Hulu/Sanbao/Dongge caves (Cheng et al., 2016) and northern hemisphere summer insolation at 65°N (Huybers, 2006). The shaded area represents the possible $MAST_{sr}$-derived temperature uncertainty introduced by the GDGT measurements (0.8°C) and the temperature calibration (1.8°C) combined. LSTs showed notable spatial differences during both the LGM and Holocene.

the spatial changes observed in the mid-Holocene and LGM on the CLP, as the two studied profiles, though geographically close, show differing temperature patterns. By inference, even if seasonal bias occurs in the brGDGT temperature proxy, such bias could not explain the different Holocene temperature patterns at the two studied profiles, as they are derived from the same proxy. Moreover, it has been proposed that in the westerly monsoon transition zone, Holocene temperature changes could be impacted by the westerlies circulation (Wu et al., 2023). However, in a relatively detailed study (J. W. Jiang et al., 2024), colder airmass did prevail in the westerlies region during the early to mid-Holocene, but the boundary is suggested to be to the west of the modern monsoon limit, and alkenone-based lake water temperature records in the transition zone show an overall Holocene cooling trend. Hence, the mid-Holocene cooling identified at the Jiyuan profile, to the east of the modern monsoon limit, could not be explained by the "westerlies" influence. Lastly, previous studies have highlighted the important role of underlying surface vegetation in regulating LSTs in arid and semi-arid regions (Lu et al., 2019). The dynamic evolution of land surface vegetation appears to be a key factor in explaining the spatial differences in temperature changes on the CLP observed in the current study.
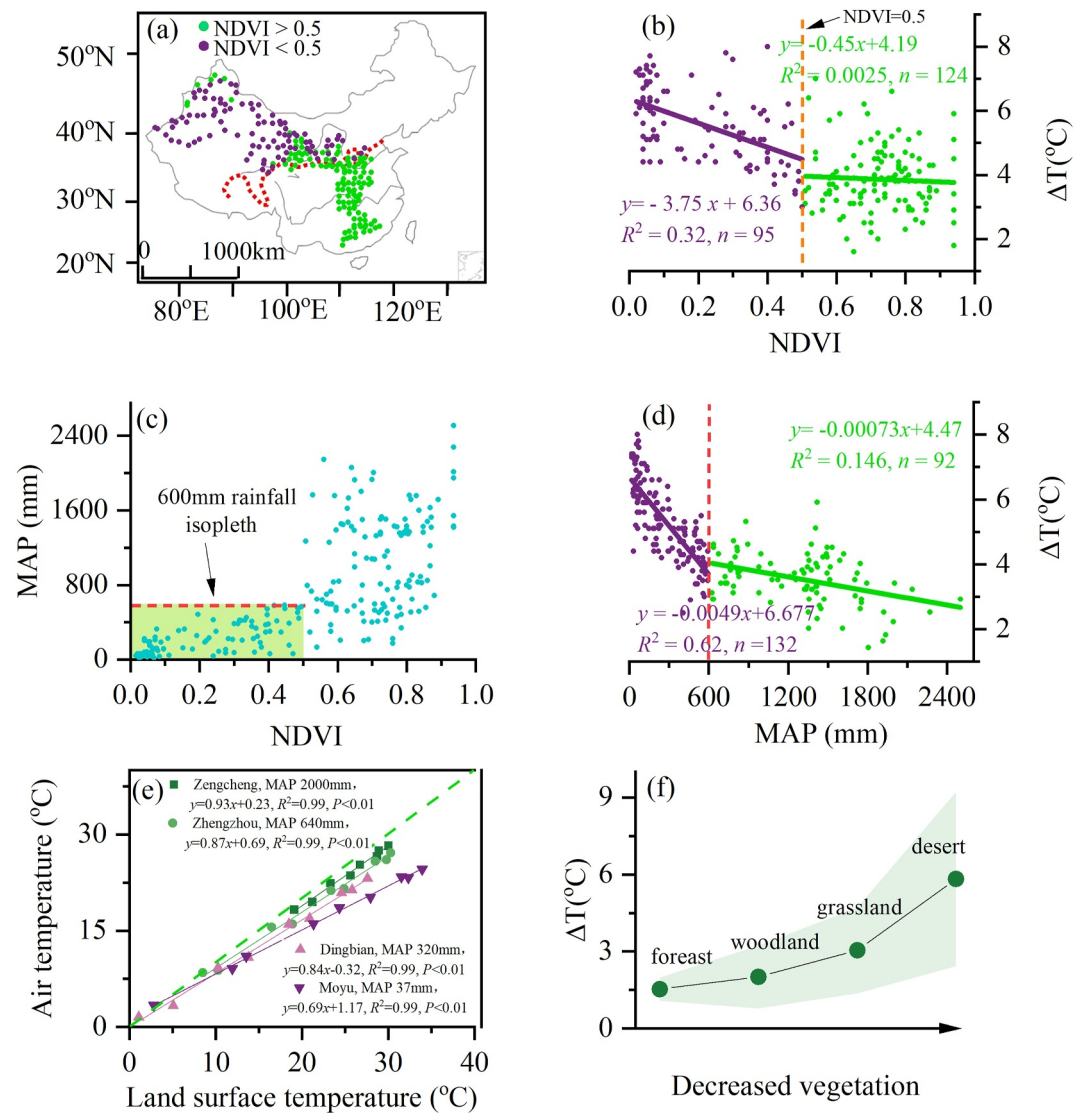
Figure 3. Vegetation-driven changes in Land surface temperatures (LSTs) on the Chinese Loess Plateau (CLP). (a) Locations of ∼200 meteorological stations in China, with the orange dashed line representing the 600 mm rainfall isopleth. (b) Correlations between the 20-year average summer LST and air temperature differences and the normalized vegetation index (NDVI) in July 2020 (Gao et al., 2023). (c) Correlations between the 20-year average mean annual precipitation (MAP) and NDVI in July 2020 (Gao et al., 2023). (d) Correlations between the 20-year average MAP and summer temperature differences between LSTs and air temperatures. (e) Comparison of air temperatures and LSTs during the bacterial growing season under different vegetation covers (forest (Zengcheng), woodland (Zhengzhou), grassland (Dingbian), and desert (Moyu)) (Lu et al., 2019). LSTs, air temperatures and MAP were obtained from the China Meteorological Administration climate records from 1981 to 2010 (http://www.cma.gov.cn).

3.2. Assessment of Vegetation Effect on LSTs

The contrasting impact of vegetation on LSTs between the Mangshan and Jiyuan sections raises an intriguing question: why does the region with better vegetation, Mangshan, exhibit a relatively weak overall impact of vegetation on LSTs (with a similar trend between LSTs and air temperatures), whereas the region with poor vegetation, Jiyuan, shows a much stronger influence of vegetation on LSTs (with decoupled temperature changes during the LGM and mid-Holocene)? To address this question, we examined the temperature difference between the LSTs and air temperatures at ∼200 meteorological stations in China, exploring their correlations with the normalized difference vegetation index (NDVI) and MAP. The key findings are as follows: (a) There is a systematic deviation between the LSTs and air temperatures, with LSTs being 2–8°C higher than air temperatures

(Figure 3). (b) There exists a threshold for the impact of vegetation on the difference between the LSTs and air temperatures. When the NDVI exceeds 0.5, the correlation between the temperature difference and vegetation is quite poor and thus the overall impact of vegetation is minor; however, when NDVI falls below 0.5, the influence of vegetation becomes more pronounced as NDVI decreases (Figure 3b). (c) When NDVI is below 0.5, the corresponding MAP typically falls below 600 mm (Figure 3c). (d) When the rainfall is less than 600 mm, the temperature difference increases noticeably as the amount of rainfall decreases (Figure 3d). In particular, we selected data from typical meteorological stations in areas with different vegetation cover (including the meteorological stations near our two profiles, Zhengzhou and Dingbian) to conduct a sensitivity analysis of vegetation's impact on the difference between LSTs and air temperatures (Figure 3 and Figure S7 in Supporting Information S1). We note that, although the LSTs and air temperatures are linearly correlated at different meteorological stations throughout the entire bacterial growing season (March to November), as indicated by H. Y. Wang et al. (2020), the slope of the correlation varied greatly (ranging from 0.69 to 0.93) (Figure 3). In areas with better vegetation cover, the LSTs and air temperatures are largely consistent, whereas in areas with poor vegetation cover, the correlation shows a substantial deviation from the 1:1 line. Further statistical analysis of these data revealed that, during the bacterial growing season, the average difference between LSTs and air temperature increased as vegetation cover decreased. The temperature differences for forest (Zengcheng), woodland (Zhengzhou), grassland (Dingbian), and desert (Moyu) areas were 1.5°C ± 0.5°C, 2.0°C ± 1.2°C, 3.0°C ± 1.7°C, and 5.8°C ± 3.4°C, respectively. In comparison, temperature differences for forested areas were typically less than 2°C and showed smaller variation, while for desert vegetation, the difference could be as high as 9.6°C. We also compared the relationship between air temperature and temperature difference in areas with different vegetation cover and found that, for the same air temperature, the difference between LSTs and air temperatures in desert vegetation areas was notably higher than in forest-covered areas (Figure S7 in Supporting Information S1). These indicated the important role of vegetation cover in regulating LSTs.

These findings highlight the complex relationship between vegetation cover, precipitation, and land surface temperature variations. Vegetation can have contrasting effects on LSTs: it may cool the surface by increasing evapotranspiration or warm it by reducing albedo (Meir et al., 2006). The net effect depends on which mechanism dominates in a region. Globally, increased vegetation generally leads to a cooling effect, except in some boreal areas (Jeong et al., 2009; Piao et al., 2020; Zeng et al., 2017). Our analysis of LST and air temperature differences suggests a net negative vegetation effect, with LSTs deviating more from air temperature in poorly vegetated regions (Figure 3 and Figure S7 in Supporting Information S1). In the absence of past NDVI data, inferring past vegetation cover changes is challenging. $\delta^{13}C_{TOC}$ from the two profiles likely reflects regional changes in vegetation type, but not necessarily vegetation cover (Figure S8 and Text S4 in Supporting Information S1). Pollen data (H. C. Jiang & Ding, 2005) indicate a notable decline in vegetation coverage from the south to north CLP but lack the temporal resolution to infer vegetation cover changes. Alternatively, a rainfall threshold of 600 mm could serve as a proxy for evaluating vegetation effects (Figure 3). Precipitation records, reconstructed from cosmogenic ^{10}Be, show that precipitation on the southern CLP was essentially greater than 600 mm, while precipitation on the north CLP was generally less than 600 mm, and could be as low as 100 mm during the glacial period (Beck et al., 2018; Zhou et al., 2007) (Figure 4). MS and TOC could serve as complementary indicators for vegetation cover changes. Both MS and TOC values in the Jiyuan profile, as compared to Mangshan (Figures S6 and S8 in Supporting Information S1), increased substantially around 8 ka, when Jiyuan LSTs started to decline. Consequently, a positive correlation between LSTs and TOC (vegetation cover) is observed at the Mangshan section, while the correlation is negative at the Jiyuan section, indicating robust negative feedback from vegetation on LST variations (Figure S9 in Supporting Information S1).

Reconstructed precipitation data suggest that the northern CLP was covered by desert vegetation during the LGM and shifted to grassland/woodland in the Holocene, while the southern CLP maintained grassland/woodland throughout (Beck et al., 2018; Zhou et al., 2007). Changes in vegetation cover could well explain the different Holocene temperature trends (Figure S6 in Supporting Information S1), as well as the early warming toward the northwestern CLP (Lu et al., 2019). Across the southern and eastern CLP, where precipitation during both glacial and interglacial periods exceeded the modern observed threshold of 600 mm, the impact of vegetation changes on LSTs was relatively small. Consequently, the difference between the LSTs and air temperatures remained relatively stable, leading to the Holocene temperature trend in the Mangshan region consistent with regional and global air temperature changes (Figure S6 in Supporting Information S1). Conversely, on the northern CLP, specifically at the Jiyuan section, despite sparse vegetation and lower soil moisture reducing albedo during the
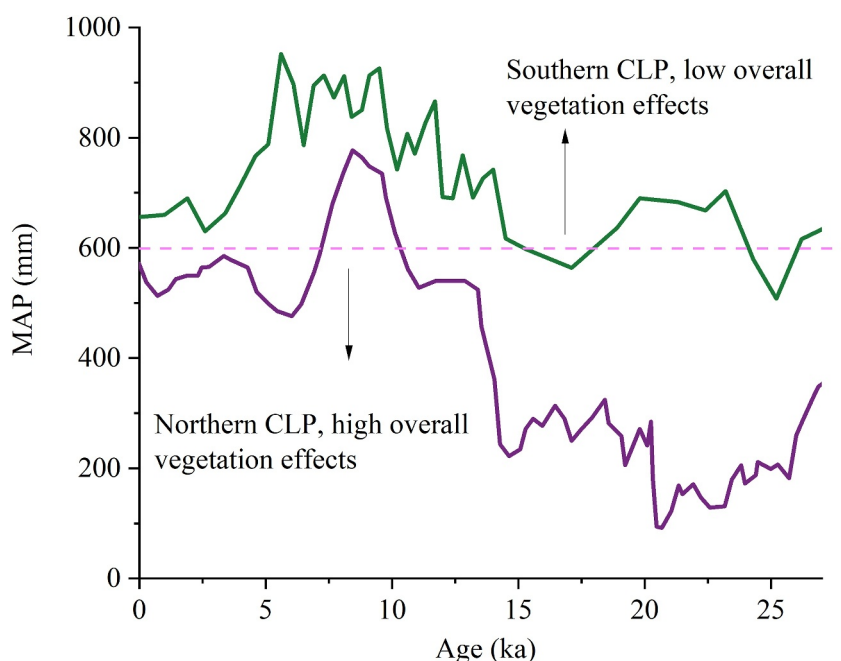
Figure 4. ^{10}Be-derived mean annual precipitation (MAP) for the southern and northern Chinese Loess Plateau (CLP) (green, Baoji, Beck et al., 2018; purple, Luochuan, Zhou et al., 2007).

LGM, decreased vegetation evaporation and lower surface heat capacity favored an increase in LSTs, leading to notable temperature disparities between LSTs and air temperatures (Figure 2). Based on a land surface energy partitioning model, even during the glacials with stronger winds, soil temperatures can still be ~5°C higher than air temperatures (Guo et al., 2024). Furthermore, in regions with sparse vegetation, temperature difference due to dynamic vegetation changes can reach 9.6°C (Figure 3). The combination of these factors led to a notable increase in LSTs during the LGM. Subsequently, from the LGM to the early Holocene, there exists a slightly increasing trend in LSTs due to rising air temperatures. However, transitioning from the early to the mid-Holocene period, an increase in rainfall triggered rapid vegetation growth. Improved vegetation covers and higher soil moisture levels enhanced the heat capacity of land surface, which, combined with the negative feedback effect of vegetation caused by enhanced evaporation, resulted in LST decline. Hence, changes in vegetation cover could have led to the divergence of trends between mid-Holocene LSTs and air temperatures at the Jiyuan section.

3.3. Implications for the Holocene Temperature Controversy

The Holocene epoch has garnered widespread attention as the most recent interglacial period, particularly in terms of temperature variations in terrestrial regions. However, discrepancies in reconstructed temperature changes have been observed across different indicators and regions (Chen et al., 2023). These differences may arise from seasonal variations reflected by different proxies or non-temperature factors (Chen et al., 2023; J. W. Jiang et al., 2024). Despite this, long-term Holocene temperature trends in mid-latitude Eurasia are generally consistent when using the same indicators, suggesting that seasonal bias can be minimized with consistent proxies (J. W. Jiang et al., 2024). Thus, while bacterial seasonal variation may contribute, it is not the primary factor for the observed differences in Holocene temperature trends. Our findings suggest that vegetation covering the land surface plays a crucial role in regulating LST changes. While air temperature trends are often assumed to be consistent within regions, past air temperature data are rarely directly accessible, as most geological materials record land or sea surface temperatures instead (Molnar, 2022). Therefore, caution is needed when interpreting proxy temperature records.

The Holocene temperature controversy could be taken as an example. Reconstructions of terrestrial Holocene temperature variations based on different temperature proxies show inconsistent spatial patterns (Cartapanis et al., 2022; J. W. Jiang et al., 2024; Kaufman et al., 2004, 2020; Li et al., 2024; Lin et al., 2024; Thompson et al., 2022; Wu et al., 2023; Zheng et al., 2025). Globally, continental proxy records from mid- and high latitudes

in the Northern Hemisphere depict a "classic" Holocene thermal maximum (HTM) (8–4 ka). In contrast, marine proxy records from the same latitudes reveal an earlier HTM (11–7 ka), while a clear temperature anomaly is absent in the tropics (Cartapanis et al., 2022). Regionally, northeastern China shows a long-term cooling trend in warm-season temperatures, while southwestern Siberia exhibits a long-term warming trend, possibly due to colder air masses prevailing in the interior of mid-latitude Eurasia during the early to mid-Holocene (J. W. Jiang et al., 2024 and references therein). Holocene temperature changes across different regions of China, based on long-chain alkenones, brGDGTs, and pollen, also exhibit considerable spatial differences within the HTM (J. W. Jiang et al., 2024; Lin et al., 2024; T. X. Wang et al., 2023; Wu et al., 2023). These records suggest a rough spatial pattern, with a relatively warm mid-Holocene and cool late Holocene in the Asian summer monsoon domain, while records from the westerlies domain show a relatively cold mid-Holocene and warm late Holocene, possibly due to the modulation of monsoon systems (Wu et al., 2023).

Our records further indicate that, within the Asian monsoon region, Holocene temperature changes reconstructed from the same type of biomarkers in different regions of the CLP also exhibit considerable spatial variability because the dynamic evolution of surface vegetation influences temperatures. On the southern CLP, the temperature maximum was observed during the mid-Holocene, whereas on the northern CLP, it occurred during the early Holocene. It underscores the need to carefully consider the impact of underlying surface features, such as vegetation, when interpreting reconstructed temperatures, as similar challenges may also arise with other proxies. Given these complexities, further investigation is essential to understand the driving mechanisms behind these variations. Continued investigations into these issues will enhance our understanding of past climate dynamics during the Holocene.

4. Conclusions

By examining temperature trends during the LGM and mid-Holocene in the two sections on the CLP with similar latitudinal and geographical characteristics but different vegetation cover, we observed substantial regional differences that could not be attributed to external common factors such as solar radiation, carbon dioxide levels, or ice sheet remnants. The disparity of Holocene LST trends, that is, an overall Holocene cooling trend on the southern CLP and mid-Holocene cooling on the northern CLP, suggests that regional vegetation cover changes played a pivotal role in shaping local LSTs patterns over time. When rainfall exceeded 600 mm, the vegetation impact on LSTs remained at a relatively low level so that LST changes closely tracked air temperature changes, allowing LSTs to serve as a reliable indicator for air temperatures. In contrast, when vegetation cover change exerts a more pronounced influence, the relationship between LSTs and air temperatures could become decoupled, highlighting the intricate interplay between vegetation dynamics and temperature trends. This study underscores the important role of vegetation cover in modulating LST changes and emphasizes the importance of considering vegetation effects when interpreting proxy temperature records.

Data Availability Statement

All GDGT data used in this study are available at Lu (2025).

References

An, Z. S., Kukla, G. J., Porter, S. C., & Xiao, J. L. (1991). Magnetic-susceptibility evidence of monsoon variation on the Loess Plateau of central China during the last 130,000 Years. *Quaternary Research*, *36*(1), 29–36. https://doi.org/10.1016/0033-5894(91)90015-w

An, Z. S., Porter, S. C., Kutzbach, J. E., Wu, X. H., Wang, S. M., Liu, X. D., et al. (2000). Asynchronous Holocene optimum of the East Asian monsoon. *Quaternary Science Reviews*, *19*(8), 743–762. https://doi.org/10.1016/s0277-3791(99)00031-1

Andersen, C., Koc, N., Jennings, A., & Andrews, J. T. (2004). Nonuniform response of the major surface currents in the Nordic Seas to insolation forcing: Implications for the Holocene climate variability. *Paleoceanography*, *19*(2), Pa2003. https://doi.org/10.1029/2002pa000873

Beck, J. W., Zhou, W. J., Li, C., Wu, Z. K., White, L., Xian, F., et al. (2018). A 550,000-year record of East Asian monsoon rainfall from [10]Be in loess. *Science*, *360*(6391), 877–881. https://doi.org/10.1126/science.aam5825

Bentley, M. J., Hodgson, D. A., Smith, J. A., Cofaigh, C. O., Domack, E. W., Larter, R. D., et al. (2009). Mechanisms of Holocene palaeoenvironmental change in the Antarctic Peninsula region. *The Holocene*, *19*(1), 51–69. https://doi.org/10.1177/0959683608096603

Bonan, G. B. (2008). Forests and climate change: Forcings, feedbacks, and the climate benefits of forests. *Science*, *320*(5882), 1444–1449. https://doi.org/10.1126/science.1155121

Bova, S., Rosenthal, Y., Liu, Z., Godad, S. P., & Mi, Y. (2021). Seasonal origin of the thermal maxima at the Holocene and the last interglacial. *Nature*, *589*(7843), 548–553. https://doi.org/10.1038/s41586-020-03155-x

Cartapanis, O., Jonkers, L., Moffa-Sanchez, P., Jaccard, S. L., & de Vernal, A. (2022). Complex spatio-temporal structure of the Holocene thermal maximum. *Nature Communications*, *13*(1), 5662. https://doi.org/10.1038/s41467-022-33362-1

Chen, F. H., Chen, J. H., Huang, W., Chen, S. Q., Huang, X. Z., Jin, L. Y., et al. (2019). Westerlies Asia and monsoonal Asia: Spatiotemporal differences in climate change and possible mechanisms on decadal to sub-orbital timescales. *Earth-Science Reviews*, *192*, 337–354. https://doi.org/10.1016/j.earscirev.2019.03.005

Chen, F. H., Duan, Y. W., Hao, S., Chen, J., Feng, X. P., Hou, J. Z., et al. (2023). Holocene thermal maximum mode versus the continuous warming mode: Problems of data-model comparisons and future research prospects. *Science China Earth Sciences*, *66*(8), 1683–1701. https://doi.org/10.1007/s11430-022-1113-x

Chen, J., Zhang, Q., Lu, Z., Duan, Y., Cao, X., Huang, J., & Chen, F. (2024). Reconciling East Asia's mid-Holocene temperature discrepancy through vegetation-climate feedback. *Science Bulletin*, *69*(15), 2420–2429. https://doi.org/10.1016/j.scib.2024.04.012

Cheng, H., Edwards, R. L., Sinha, A., Spotl, C., Yi, L., Zhang, S. R., et al. (2016). The Asian monsoon over the past 640,000 years and ice age terminations. *Nature*, *534*(7609), 640–646. https://doi.org/10.1038/nature18591

Dang, X. Y., Yang, H., Naafs, B. D. A., Pancost, R. D., & Xie, S. C. (2016). Evidence of moisture control on the methylation of branched glycerol dialkyl glycerol tetraethers in semi-arid and arid soils. *Geochimica et Cosmochimica Acta*, *189*, 24–36. https://doi.org/10.1016/j.gca.2016.06.004

Fang, X. Q., & Hou, G. L. (2011). Synthetically reconstructed Holocene temperature change in China (in Chinese). *Scientia Geographica Sinica*, *31*, 385–393.

Gao, J., Shi, Y., Zhang, H., Chen, X., Zhang, W., Shen, W., et al. (2023). China regional 250m normalized difference vegetation index data set (2000-2022). *National Tibetan Plateau Data Center*.

Gao, L., Nie, J. S., Clemens, S., Liu, W. G., Sun, J. M., Zech, R., & Huang, Y. (2012). The importance of solar insolation on the temperature variations for the past 110 kyr on the Chinese Loess Plateau. *Palaeogeography, Palaeoclimatology, Palaeoecology*, *317*, 128–133. https://doi.org/10.1016/j.palaeo.2011.12.021

Guo, B., Nie, J., Stevens, T., Buylaert, J. P., Peng, T., Xiao, W., et al. (2022). Dominant precessional forcing of the East Asian summer monsoon since 260 ka. *Geology*, *50*(12), 1372–1376. https://doi.org/10.1130/g50206.1

Guo, J., Fuchs, L., Ziegler, M., Sun, Y., & Peterse, F. (2025). Assessing tetraether lipids as a paleotemperature proxy on western edge of the Chinese Loess Plateau: A cautionary tale. *Organic Geochemistry*, *201*, 104947. https://doi.org/10.1016/j.orggeochem.2025.104947

Guo, J. J., Ziegler, M., Wanders, N., Vreeken, M., Yin, Q., Lu, Q. Z., et al. (2024). Robust land surface temperature record for North China over the past 21,000 years. *Science Advances*, *10*(8), eadj4800. https://doi.org/10.1126/sciadv.adj4800

Huybers, P. (2006). Early Pleistocene glacial cycles and the integrated summer insolation forcing. *Science*, *313*(5786), 508–511. https://doi.org/10.1126/science.1125249

Jeong, S. J., Ho, C. H., Kim, K. Y., & Jeong, J. H. (2009). Reduction of spring warming over East Asia associated with vegetation feedback. *Geophysical Research Letters*, *36*(18), L18705. https://doi.org/10.1029/2009gl039114

Jiang, H. C., & Ding, Z. L. (2005). Temporal and spatial changes of vegetation cover on the Chinese Loess Plateau through the last glacial cycle, evidence from spore-pollen records. *Review of Palaeobotany and Palynology*, *133*(1–2), 23–37. https://doi.org/10.1016/j.revpalbo.2004.08.003

Jiang, J. W., Meng, B. W., Wang, H. Y., Liu, H., Song, M., He, Y. X., et al. (2024). Spatial patterns of Holocene temperature changes over mid-latitude Eurasia. *Nature Communications*, *15*(1), 1507. https://doi.org/10.1038/s41467-024-45883-y

Kang, S. G., Du, J. H., Wang, N., Dong, J. B., Wang, D., Wang, X. L., et al. (2020). Early Holocene weakening and mid- to late Holocene strengthening of the East Asian winter monsoon. *Geology*, *48*(11), 1043–1047. https://doi.org/10.1130/g47621.1

Kaufman, D., McKay, N., Routson, C., Erb, M., Davis, B., Heiri, O., et al. (2020). A global database of Holocene paleotemperature records. *Scientific Data*, *7*(1), 115. https://doi.org/10.1038/s41597-020-0445-3

Kaufman, D. S., Ager, T. A., Anderson, N. J., Anderson, P. M., Andrews, J. T., Bartlein, P. J., et al. (2004). Holocene thermal maximum in the western Arctic (0-180ºW). *Quaternary Science Reviews*, *23*(5–6), 529–560.

Li, W., Zhang, W., & Wang, Y. (2024). Holocene seasonal temperature reconstruction based on branched glycerol dialkyl glycerol tetraethers (brGDGTs) records from different regions in China. *The Holocene*, *35*(3), 249–258. https://doi.org/10.1177/09596836241297658

Li, Y., Liu, Y., Ye, W. T., Xu, L. M., Zhu, G. R., Zhang, X., & Zhang, C. (2018). A new assessment of modern climate change, China-An approach based on paleo-climate. *Earth-Science Reviews*, *177*, 458–477. https://doi.org/10.1016/j.earscirev.2017.12.017

Lin, T. Y., Rao, Z. G., Zeng, Y. Y., Li, Y. X., Zhao, L., Liu, L. D., et al. (2024). Sedimentary brGDGTs in China: An overview of modern observations and proposed land Holocene paleotemperature records. *Earth-Science Reviews*, *250*, 104694. https://doi.org/10.1016/j.earscirev.2024.104694

Lu, H. X. (2025). brGDGTs in Mangshan and Jiyuan [Dataset]. *figshare*. https://doi.org/10.6084/m9.figshare.28122740.v1

Lu, H. X., Liu, W. G., Yang, H., Leng, Q., Liu, Z. H., Cao, Y. N., et al. (2022). Decoupled land and ocean temperature trends in the early-middle Pleistocene. *Geophysical Research Letters*, *49*(17), e2022GL099520. https://doi.org/10.1029/2022gl099520

Lu, H. X., Liu, W. G., Yang, H., Wang, H. Y., Liu, Z. H., Leng, Q., et al. (2019). 800-kyr land temperature variations modulated by vegetation changes on Chinese Loess Plateau. *Nature Communications*, *10*(1), 1958. https://doi.org/10.1038/s41467-019-09978-1

Marchal, O., Cacho, I., Stocker, T. F., Grimalt, J. O., Calvo, E., Martrat, B., et al. (2002). Apparent long-term cooling of the sea surface in the northeast Atlantic and Mediterranean during the Holocene. *Quaternary Science Reviews*, *21*(4–6), 455–483. https://doi.org/10.1016/s0277-3791(01)00105-6

Marcott, S. A., Shakun, J. D., Clark, P. U., & Mix, A. C. (2013). A reconstruction of regional and global remperature for the past 11,300 years. *Science*, *339*(6124), 1198–1201. https://doi.org/10.1126/science.1228026

Meir, P., Cox, P., & Grace, J. (2006). The influence of terrestrial ecosystems on climate. *Trends in Ecology & Evolution*, *21*(5), 254–260. https://doi.org/10.1016/j.tree.2006.03.005

Molnar, P. (2022). Differences between soil and air temperatures, Implications for geological reconstructions of past climate. *Geosphere*, *18*(2), 800–824. https://doi.org/10.1130/ges02448.1

Peterse, F., Martinez-Garcia, A., Zhou, B., Beets, C. J., Prins, M. A., Zheng, H. B., & Eglinton, T. I. (2014). Molecular records of continental air temperature and monsoon precipitation variability in East Asia spanning the past 130,000 years. *Quaternary Science Reviews*, *83*, 76–82. https://doi.org/10.1016/j.quascirev.2013.11.001

Peterse, F., Prins, M. A., Beets, C. J., Troelstra, S. R., Zheng, H. B., Eglinton, T. I., et al. (2011). Decoupled warming and monsoon precipitation in East Asia over the last deglaciation. *Earth and Planetary Science Letters*, *301*(1–2), 256–264. https://doi.org/10.1016/j.epsl.2010.11.010

Petit, J., Jouzel, J., Raynaud, D., Barkov, N. I., Basile, I., Bender, M., et al. (1999). Climate and atmospheric history of the past 420,000 years from the Vostok ice core, Antarctica. *Nature*, *399*(6735), 429–436. https://doi.org/10.1038/20859

Piao, S. L., Wang, X. H., Park, T., Chen, C., Lian, X., He, Y., et al. (2020). Characteristics, drivers and feedbacks of global greening. *Nature Reviews Earth & Environment*, *1*(1), 14–27. https://doi.org/10.1038/s43017-019-0001-x

Piao, S. L., Zhang, X. Z., Wang, T., Liang, E. Y., Wang, S. P., Zhu, J. T., et al. (2019). Responses and feedback of the Tibetan Plateau's alpine ecosystem to climate change (in Chinese). *Chinese Science Bulletin*, *64*, 2842–2855.

Shen, M. G., Piao, S. L., Jeong, S. J., Zhou, L. M., Zeng, Z. Z., Ciais, P., et al. (2015). Evaporative cooling over the Tibetan Plateau induced by vegetation growth. *Proceedings of the National Academy of Sciences of the United States of America*, *112*(30), 9299–9304. https://doi.org/10.1073/pnas.1504418112

Tang, C. Y., Yang, H., Pancost, R. D., Griffiths, M. L., Xiao, G. Q., Dang, X. Y., & Xie, S. (2017). Tropical and high latitude forcing of enhanced megadroughts in Northern China during the last four terminations. *Earth and Planetary Science Letters*, *479*, 98–107. https://doi.org/10.1016/j.epsl.2017.09.012

Thomas, E. K., Clemens, S. C., Sun, Y. B., Huang, Y. S., Prell, W., Chen, G. S., et al. (2017). Midlatitude land surface temperature impacts the timing and structure of glacial maxima. *Geophysical Research Letters*, *44*(2), 984–992. https://doi.org/10.1002/2016gl071882

Thompson, A. J., Zhu, J., Poulsen, C. J., Tierney, J. E., & Skinner, C. B. (2022). Northern Hemisphere vegetation change drives a Holocene thermal maximum. *Science Advances*, *8*(15), eabj6535. https://doi.org/10.1126/sciadv.abj6535

Wang, H. Y., An, Z. S., Lu, H. X., Zhao, Z. H., & Liu, W. G. (2020). Calibrating bacterial tetraether distributions towards in situ soil temperature and application to a loess-paleosol sequence. *Quaternary Science Reviews*, *231*, 106172. https://doi.org/10.1016/j.quascirev.2020.106172

Wang, S. W., & Gong, D. Y. (2000). Temperature changes during several special periods of the Holocene in China (in Chinese). *Progress in Natural Science*, *10*, 325–332.

Wang, T. X., Wu, D., Wang, T., Chen, L., Guo, S. L., Li, Y. M., & Zhang, C. (2023). Holocene temperature variation recorded by branched glycerol dialkyl glycerol tetraethers in a loess-paleosol sequence from the north-eastern Tibetan Plateau. *Frontiers of Earth Science*, *17*(4), 1012–1025. https://doi.org/10.1007/s11707-023-1094-6

Weijers, J. W. H., Schouten, S., Hopmans, E. C., Geenevasen, J. A. J., David, O. R. P., Coleman, J. M., et al. (2006). Membrane lipids of mesophilic anaerobic bacteria thriving in peats have typical archaeal traits. *Environmental Microbiology*, *8*(4), 648–657. https://doi.org/10.1111/j.1462-2920.2005.00941.x

Weijers, J. W. H., Schouten, S., van den Donker, J. C., Hopmans, E. C., & Sinninghe Damsté, J. S. (2007). Environmental controls on bacterial tetraether membrane lipid distribution in soils. *Geochimica et Cosmochimica Acta*, *71*(3), 703–713. https://doi.org/10.1016/j.gca.2006.10.003

Wu, J., Shen, C., Yang, H., Qian, S., & Xie, S. (2023). Holocene temperature variability in China. *Quaternary Science Reviews*, *312*, 108184. https://doi.org/10.1016/j.quascirev.2023.108184

Xin, Z. B., Xu, J. X., & Zheng, W. (2008). Spatiotemporal variations of vegetation cover on the Chinese Loess Plateau (1981–2006), Impacts of climate changes and human activities. *Science in China - Series D: Earth Sciences*, *51*(1), 67–78. https://doi.org/10.1007/s11430-007-0137-2

Yang, X. P., Scuderi, L., Paillou, P., Liu, Z. T., Li, H. W., & Ren, X. Z. (2011). Quaternary environmental changes in the drylands of China—A critical review. *Quaternary Science Reviews*, *30*(23–24), 3219–3233. https://doi.org/10.1016/j.quascirev.2011.08.009

Zeng, Z. Z., Piao, S. L., Li, Z. X., Zhou, L. M., Ciais, P., Wang, T., et al. (2017). Climate mitigation from vegetation biophysical feedbacks during the past three decades. *Nature Climate Change*, *7*(6), 432–436. https://doi.org/10.1038/nclimate3299

Zheng, Y., Liu, Z., Zheng, W., & Liu, H. (2025). Northern hemisphere mid-latitudes as a key region for reconciling the Holocene temperature conundrum. *Quaternary Science Reviews*, *347*, 109090. https://doi.org/10.1016/j.quascirev.2024.109090

Zheng, Y. H., Kang, S. G., Li, J. H., Yu, S., Lan, M. W., & Wang, J. Y. (2024). A sedimentary lipid biomarker record of Holocene temperature variations and drought events in northern China. *Palaeogeography, Palaeoclimatology, Palaeoecology*, *654*, 112468. https://doi.org/10.1016/j.palaeo.2024.112468

Zhou, W. J., Priller, A., Beck, J. W., Wu, Z. K., Chen, M. B., An, Z. S., et al. (2007). Disentangling geomagnetic and precipitation signals in an 80-Kyr Chinese loess record of ^{10}Be. *Radiocarbon*, *49*(1), 139–160. https://doi.org/10.1017/s0033822200041977

References From the Supporting Information

Crampton-Flood, E. D., Tierney, J. E., Peterse, F., Kirkels, F. M. S. A., & Sinninghe Damsté, J. S. (2020). BayMBT: A Bayesian calibration model for branched glycerol dialkyl glycerol tetraethers in soils and peats. *Geochimica et Cosmochimica Acta*, *268*, 142–159. https://doi.org/10.1016/j.gca.2019.09.043

De Jonge, C., Hopmans, E. C., Zell, C. I., Kim, J. H., Schouten, S., & Sinninghe Damsté, J. P. (2014). Occurrence and abundance of 6-methyl branched glycerol dialkyl glycerol tetraethers in soils, Implications for palaeoclimate reconstruction. *Geochimica et Cosmochimica Acta*, *141*, 97–112. https://doi.org/10.1016/j.gca.2014.06.013

De Jonge, C., Peterse, F., Nierop, K. G. J., Blattmann, T. M., Alexandre, M., Ansanay-Alex, S., et al. (2024). Interlaboratory comparison of branched GDGT temperature and pH proxies using soils and lipid extracts. *Geochemistry, Geophysics, Geosystems*, *25*(7), e2024GC011583. https://doi.org/10.1029/2024gc011583

Fuchs, L., Zhou, B., Magill, C., Eglinton, T. I., Sun, Y. B., & Peterse, F. (2022). Multiproxy records of temperature, precipitation and vegetation on the central Chinese Loess Plateau over the past 200,000 years. *Quaternary Science Reviews*, *288*, 107579. https://doi.org/10.1016/j.quascirev.2022.107579

Haslett, J., & Parnell, A. (2008). A simple monotone process with application to radiocarbon-dated depth chronologies. *Journal of the Royal Statistical Society - Series C: Applied Statistics*, *57*(4), 399–418. https://doi.org/10.1111/j.1467-9876.2008.00623.x

Jia, G. D., Rao, Z. G., Zhang, J., Li, Z. Y., & Chen, F. H. (2013). Tetraether biomarker records from a loess-paleosol sequence in the western Chinese Loess Plateau. *Frontiers in Microbiology*, *4*, 199. https://doi.org/10.3389/fmicb.2013.00199

Liang, J., Russell, J. M., Xie, H. C., Lupien, R. L., Si, G. C., Wang, J., et al. (2019). Vegetation effects on temperature calibrations of branched glycerol dialkyl glycerol tetraether (brGDGTs) in soils. *Organic Geochemistry*, *127*, 1–11. https://doi.org/10.1016/j.orggeochem.2018.10.010

Lisiecki, L. E., & Raymo, M. E. (2005). Pliocene-Pleistocene stack of 57 globally distributed benthic δ^{18}O records. *Paleoceanography*, *20*(1), PA1003. https://doi.org/10.1029/2004pa001071

Liu, W. G., Ning, Y. F., An, Z. S., Wu, Z. H., Lu, H. Y., & Cao, Y. (2005). Carbon isotopic composition of modern soil and paleosol as a response to vegetation change on the Chinese Loess Plateau. *Science in China (Series D)*, *48*(1), 93–99. https://doi.org/10.1360/02yd0148

Lu, H. X., Liu, W. G., Wang, H. Y., & Wang, Z. (2016). Variation in 6-methyl branched glycerol dialkyl glycerol tetraethers in Lantian loess-paleosol sequence and effect on paleotemperature reconstruction. *Organic Geochemistry*, *100*, 10–17. https://doi.org/10.1016/j.orggeochem.2016.07.006

Peaple, M. D., Beverly, E. J., Garza, B., Baker, S., Levin, N. E., Tierney, J. E., et al. (2022). Identifying the drivers of GDGT distributions in alkaline soil profiles within the Serengeti ecosystem. *Organic Geochemistry*, *169*, 104433. https://doi.org/10.1016/j.orggeochem.2022.104433

Wang, H. Y., Liu, Z. H., Zhao, H., Cao, Y. N., Hu, J., Lu, H. X., et al. (2024). New calibration of terrestrial brGDGT paleothermometer deconvolves distinct temperature responses of two isomer sets. *Earth and Planetary Science Letters*, *626*, 118497. https://doi.org/10.1016/j.epsl.2023.118497

Yamamoto, Y., Ajioka, T., & Yamamoto, M. (2016). Climate reconstruction based on GDGT-based proxies in a paleosol sequence in Japan, Postdepositional effect on the estimation of air temperature. *Quaternary International*, *397*, 380–391. https://doi.org/10.1016/j.quaint.2014.12.009

Yang, H., Pancost, R. D., Dang, X. Y., Zhou, X. Y., Evershed, R. P., Xiao, G. Q., et al. (2014). Correlations between microbial tetraether lipids and environmental variables in Chinese soils, optimizing the paleo-reconstructions in semi-arid and arid regions. *Geochimica et Cosmochimica Acta*, *126*, 49–69. https://doi.org/10.1016/j.gca.2013.10.041

Yang, S. L., Ding, Z. L., Li, Y. Y., Wang, W. Y., Jiang, X. F., & Huang, X. (2015). Warming-induced northwestward migration of the East Asian monsoon rain belt from the last glacial maximum to the mid-Holocene. *Proceedings of the National Academy of Sciences of the United States of America*, *112*(43), 13178–13183. https://doi.org/10.1073/pnas.1504688112

Zech, R., Gao, L., Tarozo, R., & Huang, Y. (2012). Branched glycerol dialkyl glycerol tetraethers in Pleistocene loess-paleosol sequences, three case studies. *Organic Geochemistry*, *53*, 38–44. https://doi.org/10.1016/j.orggeochem.2012.09.005

Zhao, J. J., Tsai, V. C., & Huang, Y. S. (2022). A nonlinear model for resolving the temperature bias of branched glycerol dialkyl glycerol tetraether (brGDGT) temperature proxies. *Geochimica et Cosmochimica Acta*, *327*, 158–169. https://doi.org/10.1016/j.gca.2022.04.022